RSC Advances

ROYAL SOCIETY OF CHEMISTRY

www.rsc.org/advances

Graphical Abstract

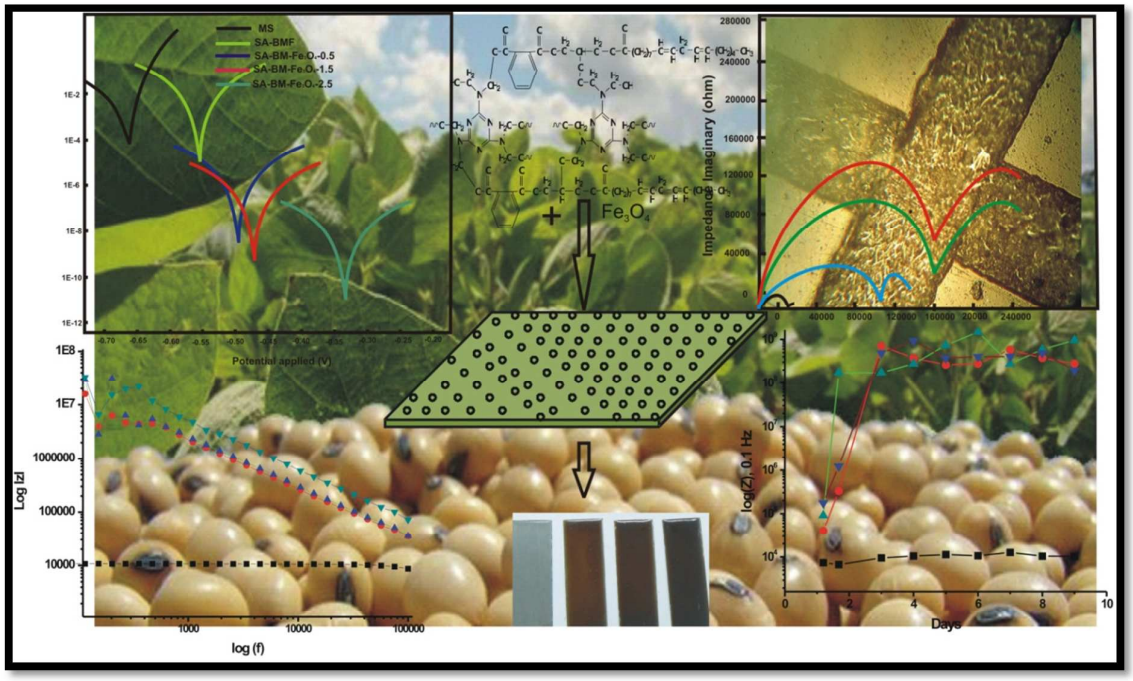

Anticorrosive nanocomposite coatings were synthesized using soya alkyd a renewable polymer matrix and Fe_3O_4 nanoparticles as filler.

Physico-mechanical and electrochemical corrosion behavior of soy alkyd/Fe_3O_4 nanocomposite coatings

Obaid ur Rahman and Sharif Ahmad*

Material Research Laboratory, Department of Chemistry, Jamia Millia Islamia, New Delhi India

Obaid ur Rahman (Senior Research Fellow)

Material Research Laboratory

Department of Chemistry

Jamia Millia Islamia, New Delhi India

obbi16@gmail.com

Dr. Sharif Ahmad* (Professor)

Material Research Laboratory

Department of Chemistry

Jamia Millia Islamia, New Delhi India

sharifahmad_jmi@yahoo.co.in

*corresponding author

Physico-mechanical and electrochemical corrosion behavior of soy alkyd/Fe_3O_4 nanocomposite coatings

Obaid ur Rahman and Sharif Ahmad*

Material Research Laboratory, Department of Chemistry, Jamia Millia Islamia, New Delhi India

Abstract

The present article reports the synthesis of butylated melamine formaldehyde (BMF) cured soy alkyd (SA-BMF) and nanoferrite (Fe_3O_4) dispersed SA-BMF (SA-BMF-Fe_3O_4) nanocomposite anticorrosive coatings. The structural elucidation of SA-BMF and SA-BMF-Fe_3O_4 was performed by Fourier transform infra-red (FT-IR) spectroscopy. Physico-mechanical properties like impact resistance, bend test, scratch hardness, cross hatch adhesion test of these coatings were analyzed by standard protocols. The thermo gravimetric analysis (TGA) was used to evaluate the thermal stability of the coating material. The corrosion resistance performance of SA-BMF and SA-BMF-Fe_3O_4 coated CS was evaluated by potentiodynamic polarization (PDP) and electrochemical impedance spectroscopy (EIS) techniques in 3.5 wt. % NaCl solution. The salt spray test for coated and uncoated carbon steel (CS) strips in 5 wt. % NaCl solution was also performed. Study revealed that the presence of Fe_3O_4 nanoparticles played a prominent role in the performance of SA-BMF matrix as reflected by high thermal stability, good hydrophobicity, enhanced physico-mechanical properties and higher corrosion resistance performance. Among different compositions, SA-BMF-Fe_3O_4-2.5 coatings exhibited far superior physico-mechanical and corrosion inhibition properties than SA-BMF coatings and other similar reported systems. The possible mechanisms of corrosion inhibition by nanocomposite coatings have also been discussed.

1. Introduction

The corrosion of materials imposes a detrimental effect on the economies of nations, which usually proceeds through the oxidation of metals and the reduction of corrosive species like that of H^+ ions, oxygen and H_2O_2. Thus, protection of materials from corrosion has become an issue of prime importance particularly in modern and advanced industrial era. Varieties of techniques have been developed to control the dynamics of corrosion.[1] Among various approaches, polymeric coatings are considered as one of the most promising.[2]

However, during the past one decade, there has been a growing interest in the development of environment friendly, cost effective, biodegradable and VOC free polymeric materials based on natural resources like natural rubber, baggase, cashewnut shell liquid, lignin, vegetable oils [VO] etc. Among various renewable resources, vegetable oils serve as a potential alternative chemical feedstock because of their many advantages like low cost, physical and chemical stability, reduced toxicity, reduced risk for handling and transportation, possibility of recycling, renewability, biodegradability, multi-functionality and environmentally benign in nature.[3] However, VO based polymeric materials do not show good strength and rigidity for industrial applications. Therefore, there is a need to modify VO based polymers to obtain useful materials finding applications in industries like inks, lubricants, adhesives paints and coatings.[4]

Among various VO based polymers alkyd has attained its production at commercial scale. Alkyd resins are oil based polyesters, widely used in the form of paints and coatings.[5] Alkyd resins possess the advantages of excellent gloss, solvent resistance and low cost due to which it acquire a unique position in paint and coating industries. However, their applications are restrained due to their low acid, water and alkaline resistance behavior. Hence, to induce the

desirable solvent and heat resistance as well as corrosion resistance properties in alkyd through various modifications become a subject of intensive research.

The development of nanoparticles and its application in the field of paints and coatings has overcome the problem of toxicity of pigments.[6, 7] Their dispersion has also improved the physico mechanical properties of polymeric vehicles such as the dispersion of inorganic nanoparticles (metal oxide) as fillers into alkyd (a polymer) matrix leading to the formation of inorganic-organic hybrid materials.[8] The hybrid materials of nano inorganic fillers and organic polymers are often called polymer nanocomposites.[9] These hybrid materials are considered as a new and versatile class of materials, offering potential applications in the field of paints and coatings.[10] The inorganic nanoparticles dispersed in polymeric vehicle fill the surface cavities if any, leading to the reduction in the surface defects like micro cracks and voids, enhancing the integrity of coatings through adhesion between coating and metal surface.[11] Further, it has been reported that the presence of low concentration (1-5%) of inorganic nanofillers in the alkyd matrix improve the physico-mechanical and corrosion protective properties of coatings.[12] Some transition metal oxide nanoparticles (like ZrO_2, ZnO, TiO_2, NiO, Fe_2O_3) which possess magnetic, electric and corrosion inhibition properties, have attracted considerable attention of the scientific community for their application as filler/pigment in polymeric coating materials.[13] However, scant literature is available on the Fe_3O_4 nanoparticles dispersed nanocomposite coatings. Recently, the effects of dispersion of ZnO,[14-18] Fe_3O_4,[19] conducting nanoparticles and carbon nanotubes[1] on various properties of polymer nanocomposites have been investigated. Haq *et al.*[20] reported bio-based nanocomposite composed of nanoclay and blend of petro and oil-based polyester. Bal *et al.*[21] prepared nanocomposites of coconut oil-based polyester and organoclay. Bio-based nanocomposites from functionalized plant oils and layered silicates have been reported by Lu *et al.*[22] Khanna *et al.*[23] have reported the electrochemical corrosion behavior of nano-iron

oxide dispersed waterborne alkyd coatings. Herein, we have made an effort to improve the corrosion protective efficiency, physico-mechanical properties and thermal stability of nanoferrite (Fe_3O_4) dispersed BMF cured soya alkyd a sustainable nanocomposite coatings. The aim of the present study is to investigate the effect of nanoparticles on physico-mechanical and electrochemical corrosion resistance performance of SA-BMF. The addition of small amount (0.5%-2.5%) of Fe_3O_4 in BMF cured soya alkyd nanocomposites remarkably improved the corrosion inhibition, scratch hardness and abrasion resistance properties of these coatings. SA-BMF-Fe_3O_4 nanocomposite coatings showed higher corrosion resistance performance than those of other reported oil based polymer nanocomposites.[15, 24]

2. Materials and Methods

2.1 Materials

Commercial soya alkyd (SA) [specific gravity (1.10), mol. Wt. (2603)] and butylated melamine formaldehyde (BMF) were procured from Shankar dyes & chemicals (Delhi, India). Ethanol (C_2H_5OH), ferrous sulphate heptahydrate ($FeSO_4.7H_2O$) was obtained from Merck (India), ethyleneglycol (HOC_2H_4OH) and ammonium hydroxide (NH_4OH) from SD fine chemicals Pvt. Ltd (Mumbai, India), hydrogen peroxide (H_2O_2 30 wt %) procured from Fisher Scientific (Mumbai, India). All the chemicals were of AR grade and used as such.

2.2 Preparation of SA-BMF and SA-BMF-Fe_3O_4 nanocomposite

Fe_3O_4 were synthesized as per our earlier reported method.[25] Briefly, metal salt precursor ferrous sulphate heptahydrate (3.00 g, 0.1008 mole) and ethylene glycol (50 mL) were taken in a 250 mL three necked flat bottomed flask, and solution was stirred under a nitrogen atmosphere for 30 min. followed by drop wise addition of 20 mL of 0.5% aqueous solution of 50% H_2O_2. The reaction was continued at 50 $^{\circ}$C for 4 hrs along with continuous stirring. The reaction mixture was maintained in a highly basic environment (pH 13.0) by the addition of 25% aqueous ammonia solution. The different wt. % of synthesised Fe_3O_4 nanoparticles

(0.5, 1.5 and 2.5 % by weight) were mixed in 10.0 g of SA-BMF resin.[26] The SA-BMF-Fe_3O_4 mixture was sonicated using ultrasonic wave sonicator at 30 ˚C for a period of 30 minutes. A homogeneous ferrite suspended colloidal solution of SA-BMF-Fe_3O_4 nanocomposite was obtained (Scheme 1). The problem of phase separation and agglomeration was observed beyond 2.5 wt. % loading of Fe_3O_4 nanoparticles in SA-BMF resin after 24 h. Hence, the loading of Fe_3O_4 nanoparticles beyond 2.5 wt% was not carried out. Finally, these nanocomposites were marked as SA-BMF-Fe_3O_4-0.5, SA-BMF-Fe_3O_4-1.5, and SA-BMF-Fe_3O_4-2.5, where the suffixes indicate the weight percentage of Fe_3O_4 nanoparticles.

2.3 Preparation and testing of coatings

The commercially available carbon steel (CS) strips. The EDX analysis of CS strips revealed the composition of the same as 2.87% C and 97.13% Fe in wt. %, hence the steel used is high carbon steel. The CS of various standard sizes were polished with different grades of SiC papers (180, 320, and 500), followed by thorough washing and rinsing with water, alcohol and acetone then dried in air. The 70 wt. % solution of SA-BMF and SA-BMF-Fe_3O_4 nanocomposite in ethanol was applied on the surface of polished and degreased CS strips by brush technique. The coatings of these materials on 70 mm × 25 mm × 1 mm size CS strips were prepared for physico-mechanical tests and 25 mm × 25 mm × 1 mm size CS strips for electrochemical corrosion tests as well as for morphological studies.

2.4 Characterization Methods

The structural elucidation of SA-BMF and SA-BMF-Fe_3O_4 was carried out by FTIR spectroscopy (IR Affinity-1 Shimadzu) using ZnSe cell (in the range of 4000 to 400 cm^{-1}). The thickness of coatings were measured by Elcometer (Model 345; Elcometer Instrument, Manchester, UK) which were found in the range of 100-150 μm The specular gloss of coatings was determined at 45˚ by gloss meter (model RSPT 20; Digital instrument, Santa Barbara, CA). Scratch hardness (BS 3900), impact resistance (101 part 5/Sec.3, 1988) and

bend test (IS ASTM-D3281-84) of plain and nanocomposite coatings were determined by standard methods. The refractive index was also determined by standard laboratory methods.[27]

Ultrasonic wave sonicator (model No. 1.5L 50H) was used at 30 °C for the homogeneous dispersion of Fe_3O_4 nanoparticles in SA-BMF matrix. Leitz Optical Microscope Model Metallux-3 was used at 100X and 200X magnifications to study the morphology of the uncorroded and corroded SA-BMF and nanocomposite coatings. The size of ferrite nanoparticles and their dispersion pattern in the polymeric matrix were investigated using transmission electron microscope (TEM) Model Philips Morgagni 268 operating at 80 KV (AIIMS, New Delhi, India). Thermogravimetric analyses (TGA) of coatings were performed using TG/DTA (Model EXSTAR TG/DTA 6000) under nitrogen atmosphere from 20 $^{\circ}$C to 800 $^{\circ}$C at heating rate of 10 $^{\circ}$C/min. Contact angles were recorded on Drop Shape Analysis System; model DSA10MK2 (Krüss GmbH, Germany) at National Physical Laboratory (NPL) New Delhi, India.

The corrosion resistance performance of SA-BMF, SA-BMF-Fe_3O_4 nanocomposite coated and uncoated CS was investigated under 3.5 wt. % NaCl, at 30 °C using a conventional three electrode cell i.e. test samples as working electrode, Pt gauge as auxiliary electrode and Ag/AgCl as reference electrode on Potentiostat/Galvanostat microAutolab type III (μ 3AVT 70762 The Netherland). The said system was supported by electrochemical software Nova 1.8 and the said software used to study the electrochemical corrosion behavior of coated and uncoated CS. The impedance and Tafel parameters were extracted by curve fitting procedure available in the software. 1.0 cm^2 area of coated and uncoated CS substrate (working electrode) were exposed to the corrosive medium by EG&G flat cell using ASTM G 59-97 methods as reported in different literatures[28-38] and the electrochemical cell also has the same area for working electrode. The electrochemical corrosion behavior of coated and uncoated

CS were taken with reference to their respective open circuit potentials (OCP), the AC (alternating-current) impedance measurements were made at open circuit potential with 20 mV amplitude of the sinusoidal voltage signal at applied frequencies in the range of 100 KHz to 0.1 Hz using ten points per decade. The polarization curves were recorded by sweeping the potential from −100 mV to +100 mV (with respect to OCP) in the noble direction at a constant scan rate of 0.005 mV/s.

The working electrodes i.e. the coated and uncoated CS were keep in the test environment for 10 min before the impedance run. This step was served to keep stabilize the electrode in a reproducible initial state and to make sure that no blistering occurred during this incubation period of electrode potential. The impedance spectra obtained for the SA-BMF and SA-BMF-Fe_3O_4 coated CS can be used to model the behavior of coated substrate by an equivalent circuit presented in Fig. 1. The Polarization resistance (R_p) of tested samples were evaluated from the slope of the potential–current plot (Tafel plots), according to the Stearn–Geary equation:[39]

$$R_p = \frac{b_a\, b_c}{2.303(b_a + b_c)\, I_{corr}} \qquad (1)$$

Here I_{corr} is the corrosion current, determined by an intersection of the linear portions of the anodic and cathodic curves, and ba and bc are anodic and cathodic Tafel slopes (ΔE/Δ log I), respectively.

The protection efficiency (P_{EF}%) was calculated by using the following equation:[39]

$$P_{EF}\% = \frac{R_P^{-1}(uncoated) - R_P^{-1}(coated)}{R_P^{-1}(coated)} \times 100\% \qquad (2)$$

Salt spray test (ASTM B 117-94) for coated SA-BMF and SA-BMF-Fe_3O_4 CS specimen was carried out for a period of 600 h in the salt mist chamber under 5 wt. % NaCl solution at 90% humidity. Scanning electron micrographs (SEM) of corroded as well as un-corroded coated

CS samples were taken on JEOL JSM840 scanning electron microscope under thin gold film at Electron Microscopy Centre (AIIMS, New Delhi India).

3. Results and discussion

Scheme 1 shows the formation of SA-BMF-Fe_3O_4 nanocomposites. During the reaction of BMF with SA, the butoxy groups of BMF reacted with hydroxyl and carboxylic groups of SA by condensation reaction leading to the formation of SA-BMF through a cross-linking reaction between their functional sites, along with the elimination of butanol. The Fe_3O_4 particles occupied the free interstitial spaces, available in the crosslinked structure of the resin leading to the formation of SA-BMF-Fe_3O_4 nanocomposite.[40, 41]

3.1 FT-IR

Fig. 2(a, b) shows the overlapped FT-IR spectra of SA-BMF and SA-BMF-Fe_3O_4, respectively. In Fig. 2a, the band at 3415.93 cm^{-1} was assigned to OH stretching absorbance whereas strong band at 1720.57 cm^{-1} may be attributed to the ester linkages present in alkyd. The bands at 2968.45 cm^{-1} and 2862.36 cm^{-1} can be ascribed to the -C-H asymmetric and symmetric stretching absorptions of the $-CH_3$ and $-CH_2$ group of fatty acid present in soya alkyd. The band at 1530.40 cm^{-1} is attributed to plane stretching of s-triazine ring of BMF introduced in SA. The presence of additional band at 1036-1073 cm^{-1} confirmed the etherification reaction of SA with BMF moiety. In Fig. 2(b) besides the above reported bands, the presence of sharp band at 586.30 cm^{-1} confirmed the inclusion of ferrite nanoparticles in SA-BMF matrix resulting in the formation of SA-BMF-Fe_3O_4 nanocomposite. However, it was observed that the basic structure of the polymer matrix remained unaffected only slight shift of IR band intensity of the characteristic absorption bands observed after incorporation of nanoparticles. It may be due to the interaction of polymer matrix with nano-Fe_3O_4 on the inclusion of Fe_3O_4 nanoparticles. [42]

3.2 Physico-mechanical properties

The physico-mechanical properties of SA-BMF and different ratios of SA-BMF-Fe_3O_4 coatings are given in Table 1. Drying to touch time (DTT) and drying to hard time (DTH) decreased on the addition of Fe_3O_4 nanoparticles in SA-BMF. The DTH further decreased on the increased loading of Fe_3O_4 in SA-BMF (Table 1). Refractive index and gloss value were also found to decrease with the increased loading of Fe_3O_4 nanoparticles, which can be attributed to the dense and opaque nature of Fe_3O_4 nanoparticles. Scratch hardness values were found to increase from 4.5 to 14.5 kg with the increased loading of Fe_3O_4 in SA-BMF matrix. The increase in scratch hardness value can be ascribed to the increase in physical interactions between polymer matrix and Fe_3O_4 nanoparticles, which restricted indentation and consequently enhanced the scratch hardness value.[43] During scratch hardness testing of coated surface, the ridges were formed along the side of scratch and no spalling of coating material was observed. This can be attributed to the enhanced plastic deformation of the nanocomposite coating. The optical micrographic analysis of SA-BMF-Fe_3O_4 (Fig. 3) confirmed that the addition of Fe_3O_4 in nanocomposite coatings improved the scratched resistance ability and adhesion at the interface of coatings and substrate surface.[44] The impact resistance of SA-BMF-Fe_3O_4 coatings was significantly improved with the addition of Fe_3O_4, which acted as a crack healer.[45] The presence of Fe_3O_4 nanoparticles in SA-BMF resin restricts the chain mobility of the SA-BMF-Fe_3O_4 coatings that enhances the impact resistance and strength of the coatings. The SA-BMF and SA-BMF-Fe_3O_4 coatings had passed the conical Mandrel bend test of 1/8 inch as characteristic of oil coatings,[46] which can be attributed to the presence of flexible aliphatic moiety and ether linkages that offer plasticizing effect in the nanocomposite coatings.[47]

3.3 Morphological Studies

The microstructures observed in optical images (Fig. 4) show the transparent nature of SA-BMF coatings, which was slightly affected by the dispersion of Fe_3O_4 in the SA-BMF matrix.

The uniform distribution of color throughout the matrix also implies that the Fe_3O_4 nanoparticles were uniformly distributed throughout the polymer matrix. The optical micrograph of SA-BMF-Fe_3O_4 also showed the increase in the colour intensity of coatings with the increased loading of Fe_3O_4 nanoparticles in nanocomposite coatings.[48, 49]

The TEM micrographs like optical micrographs exhibited dispersion of Fe_3O_4 in nanocomposite coatings. Fe_3O_4 nanoparticles (20-50 nm) were uniformly dispersed (Fig. 5) in the SA-BMF matrix, although we have earlier observed that the virgin Fe_3O_4 particles undergo agglomeration,[25] while on dispersion in SA-BMF matrix, these Fe_3O_4 particles encapsulated within the polymeric vehicle leading to the homogeneous dispersion of Fe_3O_4 particles in coatings.[50]

The SEM micrographs of SA-BMF and SA-BMF-Fe_3O_4-2.5 coated CS are given in Fig. 6 (a and b). The SEM micrograph of SA-BMF Fig. 6 (a) exhibited uniform morphology of the coating, while, the SEM micrograph of SA-BMF-Fe_3O_4-2.5 coated CS specimen Fig. 6 (b) showed the formation of closely packed, continuous, dense and uniform nano Fe_3O_4 dispersed coating. Despite being a composite nature of coating, it was observed that neither dispersion nor separation of two phases was observed, indicating intimate and homogeneous mixing of the Fe_3O_4 in SA-BMF.

3.4 Thermal analysis

The thermal degradation behavior of SA-BMF and SA-BMF-Fe_3O_4 nanocomposite cured resin is depicted in Fig. 7. The 5 wt. % loss occurred in the temperature range 180-200 $^{\circ}$C, due to the loss of imbibed solvent molecules. The first degradation (about 20 wt. %) of SA-BMF was observed at around 250 $^{\circ}$C while in case of SA-BMF-Fe_3O_4, the same was occurred at around 300 $^{\circ}$C. This weight loss can be attributed to the decrosslinking of SA-BMF. The second weight loss (60 wt. %) occurred at around 350 $^{\circ}$C in SA-BMF while in SA-BMF-Fe_3O_4, weight loss was observed at 390 $^{\circ}$C, this can be attributed to the decomposition of

ester, ether and melamine ring respectively.[51] The 100% decomposition was observed in case of SA-BMF coatings, while around 22 wt.% residue remained left (at around 800 °C) in case of SA-BMF-Fe_3O_4. The presence of 22 wt.% residue in nanocomposite confirmed that the incorporation of Fe_3O_4 enhances the thermal stability of SA-BMF coatings.[52] The improved thermal stability in SA-BMF-Fe_3O_4 can be attributed to the interaction between the polymer matrix and large surface area of nano-Fe_3O_4 particles, forming a stable nanocomposite coatings.[53]

3.5 Contact Angle

Hydrophobicity is an important characteristic, which does not allow the aqueous corrosive molecules to stick with the coating surface, conferring good anticorrosive properties of these coatings. Fig. 8 a-d shows the CCD camera images of water droplets on the smooth surface of SA-BMF and SA-BMF-Fe_3O_4 coatings surface. The contact angle values obtained (93-96) were well within the range of values (more than 90°) assigned to the typical hydrophobic surfaces, suggesting that these coatings were hydrophobic in nature.

3.6 Corrosion Studies

(a) Potentiodynamic polarization (PDP)

The potentiodynamic polarization curve for SA-BMF, SA-BMF-Fe_3O_4 nanocomposite coated CS and bare CS recorded in a 3.5 wt. % NaCl aqueous solution are shown in Fig. 9. The values of corrosion potential (E_{corr}) as well as polarization resistance (R_p) were calculated from PDP curve for SA-BMF and SA-BMF-Fe_3O_4 nanocomposite coated CS are summarized in Table 2. The E_{corr} value (with reference to Ag/AgCl electrode) increased from -669.5 mV for bare CS to -551.96 mV (SA-BMF coated CS). However, in case of ferrite dispersed SA-BMF coated CS, a reasonably high increase in E_{corr} value in comparison to that of SA-BMF coated CS was observed (Table 2). Likewise, the polarization resistance (R_p) value for SA-BMF-Fe_3O_4 coated CS show fivefold (1.05×10^5 kΩ) increase with respect to SA-BMF coated

CS (Rp= 11.06 kΩ). Hence, the inclusion of ferrite nanoparticles promisingly enhanced the corrosion resistance performance of SA-BMF, which was also evident from the high PE% of these coatings (Table 2). The enhanced anticorrosive performance of SA-BMF-Fe_3O_4 nanocomposite coated CS can be ascribed to the presence of ferrite nanoparticles. The presence of homogeneously dispersed Fe_3O_4 in SA-BMF matrix act as a strong barrier by inhibiting the diffusion of corrosive ions to the metal coating interface, thus, provide a tortuous pathway for the corrosive ions to reach the metal surface. Further, the presence of oxygen in ferrite facilitates the adhesion between coating and metal substrate. Thus, Fe_3O_4 nanoparticles protect the metal surfaces by acting as strong barrier.[11, 12]

(b) Electrochemical Impedance Spectroscopy (EIS)

Apart from PDP measurements, EIS was applied to give more detailed information on electrochemical performance and corrosion protection mechanism of SA-BMF and SA-BMF-Fe_3O_4 nanocomposite coatings along with the role of loading of Fe_3O_4 in SA-BMF i.e. 0.5, 1.5 and 2.5 wt. % (as per Scheme 2). The coated CS was exposed to 3.5 wt. % NaCl solution for a period of 9 days. Figs. 10 and 11 show the Nyquist plot (real impedance vs Imaginary impedance) and Bode plot (log frequency vs. log |Z|) respectively. The impedance value for SA-BMF after one day immersion was found below 10^4 Ω at the low-frequency end of the semicircle arc with the real axis (Fig. 10 a). The impedance arc of the Fig. 10a shows the capacitive loops formed in the high frequency region. The semicircular loops in the low frequency region are depressed owing to surface heterogeneities. On the other hand, capacitive loops formed in the high frequency region are somewhat less depressed. This indicates that the inner surface film is compact and continuous providing good protection as reported in the literature[54]. While in case of ferrite dispersed nanocomposite coatings the impedance value was observed to be having very high value more than 10^5 Ω Fig. 10 (b-c) nanocomposite coatings remarkably show higher impedance in the lowest frequency region,

which is a characteristic of intact well adhered coating systems.[55, 56] Further, with the increased loading of Fe_3O_4 nanoparticles, the diameter of the semicircle increases, which confirmed the better corrosion protection performance of the SA-BMF-Fe_3O_4 nanocomposite coatings as evident from the high impedance values observed from Bode plot Fig. 11.[35] In present case, the order of corrosion protection efficiency was found to be as follows: SA-BMF-Fe_3O_4-2.5 wt. %,> SA-BMF-Fe_3O_4-1.5 wt. %,> SA-BMF-Fe_3O_4-0.5 wt. % >SA-BMF. The SA-BMF coated sample and SA-BMF-Fe_3O_4 nanocomposite coatings continue to expose to the corrosive ions (Cl^-) for 9 days. In case of SA-BMF coatings, after the first day immersion, the diffusion impedance of coatings with respect to these ions acquiring Warburg impedance shape, which begins to dominate with increasing the immersion time suggesting that the electrolyte penetrates into the polymeric matrix, however, the presence of Fe_3O_4 nanoparticles in SA-BMF matrix impede the electrolyte at coating metal interface by acting as a strong barrier in saline environment as shown in Fig. 10 (b-c) and 11 (b-c) in comparison to SA-BMF coated CS (Fig. 10 (a) and 11 (a). In addition, the hydrophobicity of the coatings (Fig. 8) was increased with increased loading of ferrite nanoparticles, which do not allow wetting of the surface that inhibited the penetration of corrosive ions.[57] An increase in $|Z|_{0.1}$ Hz value is also associated with the strong barrier property of Fe_3O_4 nanoparticles present in the nanocomposite coatings. SA-BMF-Fe_3O_4 nanocomposite coatings showed higher impedance values at lower frequency as compared to that of SA-BMF coated CS as well as other similar reported systems.[58] The decrease in impedance values of coatings depends on the water uptake content of coatings. In case of SA-BMF-Fe_3O_4 nanocomposite coatings only one capacitive time constant was detected in EIS experiment after 9 days immersion in 3.5 wt. % NaCl solution (Fig. 11 b-c). This indicates that the corrosion process has not been initiated on the substrate and the nanocomposite coatings still prevent the underlying metal to come in direct contact with the aqueous corrosive environment.

The log |Z| vs time plots (Fig. 12) are widely used to compare the impedance value for the corrosion resistance performance, even without knowing the exact mechanism of the corrosion resistance performance of proposed coating systems.[57] The plot between log |Z| verses time at 0.1 Hz exhibit an increase in the value of log |Z| with time support the higher corrosion protection behavior of nanocomposite coatings, which was also evident from potentiodynamic polarization plots exhibiting higher E_{corr} values (higher corrosion resistance). The plots (Fig. 12) of logarithm of impedance modulus (log |Z|) versus time at selected frequency (0.1 Hz) were developed for these systems immersed in 3.5 wt. % of NaCl solution for nine days. The impedance spectra for SA-BMF and SA-BMF-Fe_3O_4 nanocomposite coated samples with different loading of nanoparticles (0.5%, 1.5% and 2.5%) in nanocomposite coatings were compared. Higher impedance values were observed in case of nanocomposite coatings, which was in accordance to that of PDP plots (Fig. 9), which showed higher corrosion protection efficiency of nanocomposite coatings. The higher increased in the log |Z| values (more than 10^7 Ω); indicate the better barrier properties i.e. good corrosion protection efficiency of these coatings. Hence, superior corrosion resistance performance of SA-BMF-Fe_3O_4 can be attributed to the presence of nanoparticles in the free interstitial spaces of matrix behave as strong barrier at coating-metal interface. The present investigations suggest that the presence of Fe_3O_4 nanoparticles in SA-BMF resin provide higher impedance value, led to the higher corrosion protective performance for a longer period.

(c) Salt mist test

The SA-BMF, SA-BMF-Fe_3O_4-0.5, SA-BMF-Fe_3O_4-1.5, and SA-BMF-Fe_3O_4-2.5 coatings withstand upto 11, 13 , 22 and 32 days respectively without any spalling of coating material in presence of salt solution under fog test performed in 5.0 wt. % NaCl solution under 90% humidity. The corrosion protection efficiency of these coatings was found to increase with

the increased loading of Fe_3O_4 nanoparticles. The higher corrosion protection efficiency of SA-BMF-Fe_3O_4 in saline environment can be attributed to the uniform and homogeneous dispersion of nano Fe_3O_4 particles in the nanocomposite coatings that provided a strong barrier layer at metal coating interface, which enhances the corrosion protective ability of nanocomposite coatings.[59]

(d) **Cross hatch test after corrosion**

Fig. 13 shows the optical micrographs of the scratched tested surface after corrosion test, which show no evidence of separation of coatings (Fig. 13 a-d) that confirmed the strong adhesion between SA-BMF-Fe_3O_4 coatings and CS surface. It is very interesting to note that the after the corrosion test, coatings remain well adhered with the CS substrate. This result clearly indicate that there is a strong adhesion between the nanocomposite coating material and metal substrate, which is also clearly visible in the optical micrograph. After corrosion test, only fading in colour of the coating was observed.

3.7 Scanning electron microscopy (SEM)

The SEM micrographs of SA-BMF and SA-BMF-Fe_3O_4-2.5 coated CS are given in Fig. 14. Fig. 14 c show the surface of CS substrate before corrosion test. The SEM micrograph of 5.0 wt. % of NaCl corroded SA-BMF coated CS specimen (Fig. 14 a) showed the formation of blisters and pin holes and after removing the coating from CS, SEM image (Fig. 14 e) show the damage in the CS substrate but the damage in the CS substrate as compare to uncoated CS (Fig. 14 c) is less which show that SA-BMF protect the surface at some extent. While in case of SA-BMF-Fe_3O_4-2.5 coatings even after 600 h exposure in 5.0 wt. % NaCl, the coatings showed no evidence of blister and pinholes but have a slight deposition of salt on its surface, and the coating was remained intact with the metal surface (Fig. 14 b) which was further supported by the SEM image (Fig. 14 f) of tested sample of SA-BMF-Fe_3O_4-2.5 coated CS after the removal of coatings. It can be attributed to the dense and continuous

structure of nanocomposite coating that enhanced the ability of the coatings to protect the substrate.

3.8 Corrosion mechanism

The corrosion inhibition mechanism of nanocomposite coatings is discussed as per Scheme 2. The SA-BMF-Fe_3O_4 nanocomposite coatings provide protection to the metal substrate in the following ways (i) the presence of pendant polar functionalities in coatings induces strong electrostatic interactions between the coating material and metal surface leading to the formation of well adhered and compact coating on the metal surface, followed by (ii) the presence of Fe_3O_4 nanoparticles in SA-BMF act as strong barrier for corrosive ion at the metal-coating interface, (iii) the presence of Fe_3O_4 nanoparticles within the coating material as a filler provide locking effect at the interstitial spaces and other coating artifacts (micro cracks and voids), which induce healing effect to the coating material. Hence, the protection mechanism for SA-BMF-Fe_3O_4 nanocomposite coatings were governed by adhesion, barrier and locking effect of nanofillers, which inhibit the corrosion, and enhances the corrosion-protection efficiency of SA-BMF-Fe_3O_4 nanocomposite coatings, which is also evident from PDP, EIS and salt spray test (Fig. 9, Fig. 10 and Fig. 11).

The SEM micrographs of salt spray test shows no evidence of cracks, pits or bristle formation (Fig.14 b). Further, removal of coating after salt spray test, show no evidence of penetration of corrosive ions at the substrate surface (Fig. 14 f), this also confirms the strong protective behavior of the nanocomposite coatings.

4. Conclusion

The nanocomposite coatings were synthesized using different loadings of Fe_3O_4 nanoparticles in SA-BMF matrix. The nanocomposite coatings are eco-friendly in nature as they are found to be VOC free, exhibited remarkably higher physico-mechanical properties and electrochemical corrosion resistance performance in saline environment. The inclusion of

ferrite nanoparticles significantly enhanced the physico-mechanical properties. The effective anticorrosion behavior of nanocomposite coating was confirmed by the higher protection efficiency of these coatings. The nanocomposite coating also exhibits good stability in a salt fog environment with no degradation of the coating occurring over a long immersion time. The presence of Fe_3O_4 particles also provides good locking effect by filling the coating artifacts, leading to the enhancement in the corrosion resistance performance and durability of nanocomposite coatings. Among different compositions of nanocomposite coatings, SA-BMF-Fe_3O_4-2.5 wt. % dispersion exhibited more compact, uniform coatings having good physico-mechanical properties and remarkably higher corrosion resistance properties.

Acknowledgements

One of the authors is thankful to CSIR, India (Obaid ur Rahman) for financial support in the form of CSIR senior research fellowship (vide grant No: 9/466 (0164) 2K13-EMR-I). The authors acknowledge the 'Sophisticated Analytical Instrumentation Facility (SAIF)'centre, All India Institutes of Medical Sciences (AIIMS), New Delhi for TEM and SEM facility, and are also grateful to NRB India project (No. DNRD/05/400B/155) for providing the Potentiostat/Galvanostat microAutolab facilities to carry out the PDP and EIS studies.

References

1. Z. Guo, H. Wei, D. Ding and S. Wei, *J. Mater. Chem. A*, 2013.
2. A. E. Hughes, I. S. Cole, T. H. Muster and R. J. Varley, *NPG Asia Materials*, 2010, **2**, 143-151.
3. S. Miao, P. Wang, Z. Su and S. Zhang, *Acta Biomaterialia*, 2013.
4. S. Pathan and S. Ahmad, *J. Mater. Chem. A*, 2013.
5. D. İşeri-Çağlar, E. Baştürk, B. Oktay and M. V. Kahraman, *Progress in Organic Coatings*, 2013.
6. M. Martí, L. Molina, C. Alemán and E. Armelin, *ACS Sustainable Chemistry & Engineering*, 2013.
7. J. Rawat, S. Ray, P. Rao and N. V. Choudary, Materials Science Forum, 2010.
8. C. Sanchez, P. Belleville, M. Popall and L. Nicole, *Chemical Society Reviews*, 2011, **40**, 696-753.
9. J. R. Potts, D. R. Dreyer, C. W. Bielawski and R. S. Ruoff, *Polymer*, 2011, **52**, 5-25.
10. G. Kickelbick, *Progress in Polymer Science*, 2003, **28**, 83-114.
11. X. Shi, T. A. Nguyen, Z. Suo, Y. Liu and R. Avci, *Surface and Coatings Technology*, 2009, **204**, 237-245.
12. T.-C. Huang, Y.-A. Su, T.-C. Yeh, H.-Y. Huang, C.-P. Wu, K.-Y. Huang, Y.-C. Chou, J.-M. Yeh and Y. Wei, *Electrochimica Acta*, 2011, **56**, 6142-6149.
13. A. Mathiazhagan and R. Joseph.

14. M. Kathalewar, A. Sabnis and G. Waghoo, *Progress in Organic Coatings*, 2013.
15. S. K. Dhoke, A. Khanna and T. Sinha, *Progress in Organic Coatings*, 2009, **64**, 371-382.
16. J. Alam, U. Riaz, S. M. Ashraf and S. Ahmad, *J. Coat. Technol. Res.*, 2008, **5**, 123-128.
17. F. Gojny, M. Wichmann, U. Köpke, B. Fiedler and K. Schulte, *Composites Science and Technology*, 2004, **64**, 2363-2371.
18. B. Bhanvase and S. Sonawane, *Chemical Engineering Journal*, 2010, **156**, 177-183.
19. J. Zheng, Y. Dong, W. Wang, Y. Ma, J. Hu, X. Chen and X. Chen, *Nanoscale*, 2013, **5**, 4894-4901.
20. M. Haq, R. Burgueño, A. K. Mohanty and M. Misra, *Composites Science and Technology*, 2008, **68**, 3344-3351.
21. A. Bal, G. Güçlü, I. Acar and T. B. İyim, *Progress in Organic Coatings*, 2010, **68**, 363-365.
22. J. Lu, C. K. Hong and R. P. Wool, *Journal of Polymer Science Part B: Polymer Physics*, 2004, **42**, 1441-1450.
23. S. K. Dhoke and A. Khanna, *Materials Chemistry and Physics*, 2009, **117**, 550-556.
24. J. Alam, U. Riaz, S. Ashraf and S. Ahmad, *Journal of Coatings Technology and Research*, 2008, **5**, 123-128.
25. O. u. Rahman, S. C. Mohapatra and S. Ahmad, *Materials Chemistry and Physics*, 2012, **132**, 196-202.
26. S. Ahmad, U. Riaz, M. Kashif and M. S. Khan, *J. Appl. Polym. Sci.*, 2012, **124**, 365-372.
27. E. Sharmin, D. Akram, F. Zafar, S. M. Ashraf and S. Ahmad, *Prog. Org. Coat.*, 2012, **73**, 118-122.
28. C.-W. Peng, K.-C. Chang, C.-J. Weng, M.-C. Lai, C.-H. Hsu, S.-C. Hsu, S.-Y. Li, Y. Wei and J.-M. Yeh, *Polymer Chemistry*, 2013, **4**, 926-932.
29. T. Tüken, G. Arslan and M. Erbil, *Corrosion Science*, 2004, **46**, 2743-2754.
30. M. Campo, M. Carboneras, M. López, B. Torres, P. Rodrigo, E. Otero and J. Rams, *Surface and Coatings Technology*, 2009, **203**, 3224-3230.
31. *Annu. Book ASTM Stand. 03.02, Section 3*, 2001.
32. T.-I. Yang, C.-W. Peng, Y. L. Lin, C.-J. Weng, G. Edgington, A. Mylonakis, T.-C. Huang, C.-H. Hsu, J.-M. Yeh and Y. Wei, *Journal of Materials Chemistry*, 2012, **22**, 15845-15852.
33. T. Zafeiropoulou, E. Rakanta and G. Batis, *Progress in Organic Coatings*, 2011, **72**, 175-180.
34. D. B. Hmamou, R. Salghi, A. Zarrouk, H. Zarrok, S. Al-Deyab, O. Benali and B. Hammouti, *Int. J. Electrochem. Sci*, 2012, **7**, 8988-9003.
35. C.-J. Weng, J.-Y. Huang, K.-Y. Huang, Y.-S. Jhuo, M.-H. Tsai and J.-M. Yeh, *Electrochimica Acta*, 2010, **55**, 8430-8438.
36. S. H. Sonawane, B. M. Teo, A. Brotchie, F. Grieser and M. Ashokkumar, *Industrial & Engineering Chemistry Research*, 2010, **49**, 2200-2205.
37. S. Kozhukharov, V. Kozhukharov, M. Wittmar, M. Schem, M. Aslan, H. Caparrotti and M. Veith, *Progress in Organic Coatings*, 2011, **71**, 198-205.
38. D. K. Yadav, D. Chauhan, I. Ahamad and M. Quraishi, *RSC Advances*, 2013, **3**, 632-646.
39. T.-C. Yeh, T.-C. Huang, H.-Y. Huang, Y.-P. Huang, Y.-T. Cai, S.-T. Lin, Y. Wei and J.-M. Yeh, *Polymer Chemistry*, 2012, **3**, 2209-2216.
40. S. Ahmad, S. M. Ashraf, G. S. Kumar, A. Hasnat and E. Sharmin, *Prog. Org. Coat.*, 2006, **56**, 207-213.
41. F. J. Hahn, Google Patents, Editon edn., 1950.
42. S. K. Dhoke and A. Khanna, *Corrosion Science*, 2009, **51**, 6-20.
43. J. Sanes, F. Carrión and M. Bermúdez, *Wear*, 2010, **268**, 1295-1302.
44. S. K. Dhoke, R. Bhandari and A. S. Khanna, *Progress in Organic Coatings*, 2009, **64**, 39-46.
45. B. Wetzel, F. Haupert and M. Qiu Zhang, *Composites Science and Technology*, 2003, **63**, 2055-2067.
46. E. Sharmin, S. Ashraf and S. Ahmad, *International journal of biological macromolecules*, 2007, **40**, 407-422.

47. B. De and N. Karak, *Journal of Materials Chemistry A*, 2013, **1**, 348-353.
48. O. Becker, R. Varley and G. Simon, *Polymer*, 2002, **43**, 4365-4373.
49. J. George, V. A. Sajeevkumar, K. V. Ramana and S. N. Sabapathy, *Journal of Materials Chemistry*, 2012, **22**, 22433-22439.
50. C. Sun, J. S. Lee and M. Zhang, *Advanced drug delivery reviews*, 2008, **60**, 1252-1265.
51. S. Pathan and S. Ahmad, *ACS Sustainable Chemistry & Engineering*, 2013.
52. D. Chattopadhyay and D. C. Webster, *Progress in Polymer Science*, 2009, **34**, 1068-1133.
53. S. K. Dhoke, R. Bhandari and A. Khanna, *Progress in Organic Coatings*, 2009, **64**, 39-46.
54. N. Mahato and M. Singh, *Portugaliae Electrochimica Acta*, 2011, **29**, 233-251.
55. M. Heidarian, M. Shishesaz, S. Kassiriha and M. Nematollahi, *Progress in Organic Coatings*, 2010, **68**, 180-188.
56. S. Touzain, Q. L. Thu and G. Bonnet, *Progress in Organic Coatings*, 2005, **52**, 311-319.
57. K. Schaefer and A. Miszczyk, *Corrosion Science*, 2013, **66**, 380-391.
58. S. K. Dhoke and A. Khanna, *Progress in Organic Coatings*, 2012, **74**, 92-99.
59. H. Shi, F. Liu, L. Yang and E. Han, *Progress in Organic Coatings*, 2008, **62**, 359-368.

Captions

Figures

Scheme 1 Synthesis of SA-BMF-Fe_3O_4 nanocomposite coatings

Fig. 1 Electrochemical circuit fit in the EIS studies

Fig. 2 FTIR spectra of: (a) SA-BMF and (b) SA-BMF-Fe_3O_4-2.5

Fig. 3 Optical images of scratched CS coated with (a) SA-BMF, (b) SA-BMF-Fe_3O_4-0.5, (c) SA-BMF-Fe_3O_4-1.5 and (d) SA-BMF-Fe_3O_4-2.5 at 100× before corrosion test and (e) SA-BMF, (f) SA-BMF-Fe_3O_4-0.5, (g) SA-BMF-Fe_3O_4-1.5 and (h) SA-BMF-Fe_3O_4-2.5 at 200× after corrosion test

Fig. 4 Optical images of: (a) SA-BMF, (b) SA-BMF-Fe_3O_4-0.5, (c) SA-BMF-Fe_3O_4-1.5 and (d) SA-BMF-Fe_3O_4-2.5

Fig. 5 TEM micrographs of SA-BMF-Fe_3O_4-2.5

Fig. 6 SEM micrograph of (a) SA-BMF and (b) SA-BMF-Fe_3O_4 nanocomposite

Fig. 7 TGA thermogram of: (a) SA-BMF and (b) SA-BMF-Fe_3O_4-2.5

Fig. 8 Contact angle images of: (a) SA-BMF, (b) SA-BMF-Fe_3O_4-0.5, (c) SA-BMF-Fe_3O_4-1.5 and (d) SA-BMF-Fe_3O_4-2.5

Fig. 9 Potentiodynamic polarization curve

Fig. 10 Nyquist plot in 3.5 wt. % NaCl solution of: (a) SA-BMF (b) SA-BMF-Fe_3O_4-0.5 (c) SA-BMF-Fe_3O_4-1.5, (d) SA-BMF-Fe_3O_4-2.5

Fig. 11 Bode plot in 3.5 wt. % NaCl solution of SA-BMF and nanocomposite coated samples (a) SA-BMF (b) BMF-Fe_3O_4-0.5(c) SA-BMF-Fe_3O_4-1.5 (d) BMF-Fe_3O_4-2.5

Fig. 12 $\log|Z|_{0.1Hz}$ vs exposure time for SA-BMF and SA-BMF-Fe_3O_4 nanocomposite coated samples during exposure to 3.5 wt. % NaCl

Fig. 13 (a) SA-BMF, (a) SA-BMF-Fe_3O_4-0.5, (c) SA-BMF-Fe_3O_4-1.5 and (d) SA-BMF-Fe_3O_4-2.5 at 200× after corrosion test

Fig. 14 SEM Images after corrosion test: (a) SA-BMF coated after 25 days, (b) SA-BMF-Fe_3O_4-2.5 coated after 25 days (c) CS uncorroded, (d) CS Corroded after 25 days, (e) SA-BMF corroded CS after removal of coating after 25 days and (e) SA-BMF-Fe_3O_4-2.5 after removal of coating after 25 days

Scheme 2 Mechanism of corrosion inhibition by nanocomposite coatings

Tables

Table 1 Physico-mechanical properties of SA-BMF and SA-BMF- Fe_3O_4 coatings

Table 2 Corrosion resistance performance by Potentiodynamic measurements of coatings

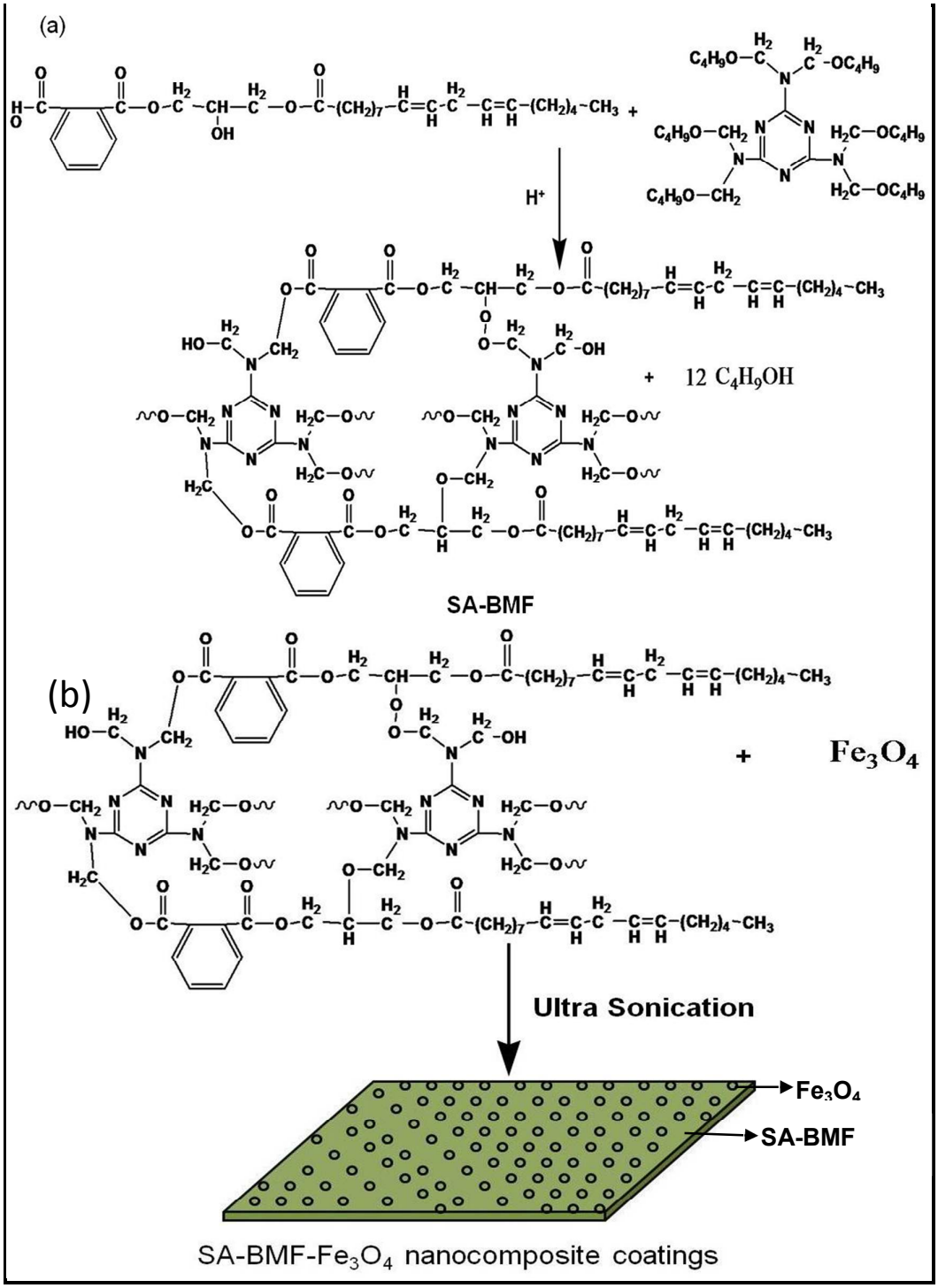

Scheme 1 Synthesis of SA-BMF-Fe_3O_4 nanocomposite coatings

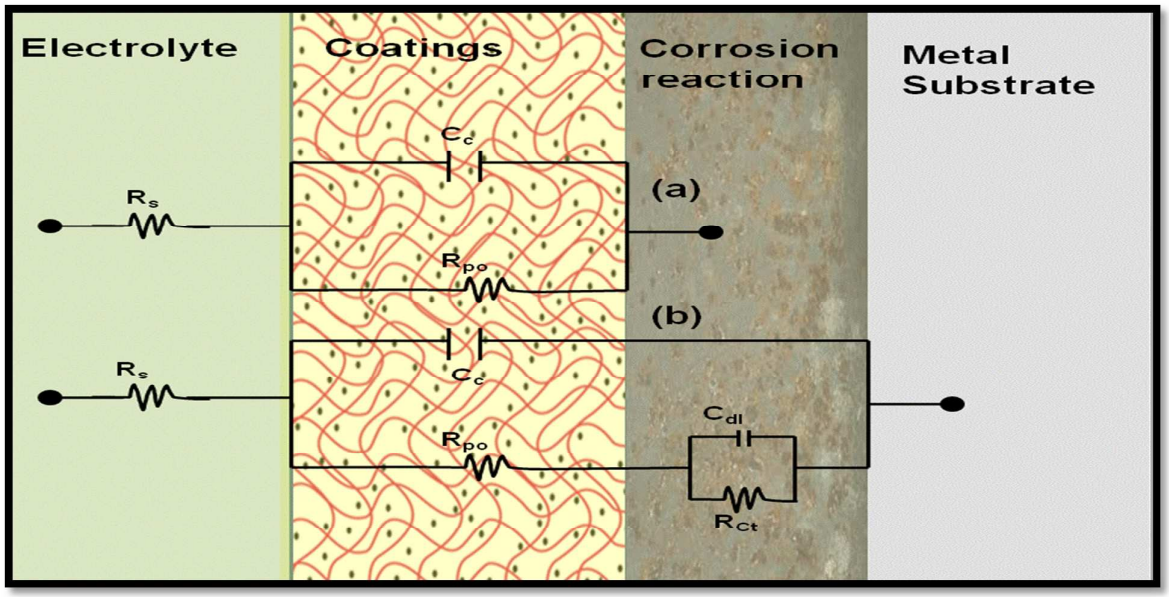

Fig. 1 Electrochemical circuit fit in the EIS studies

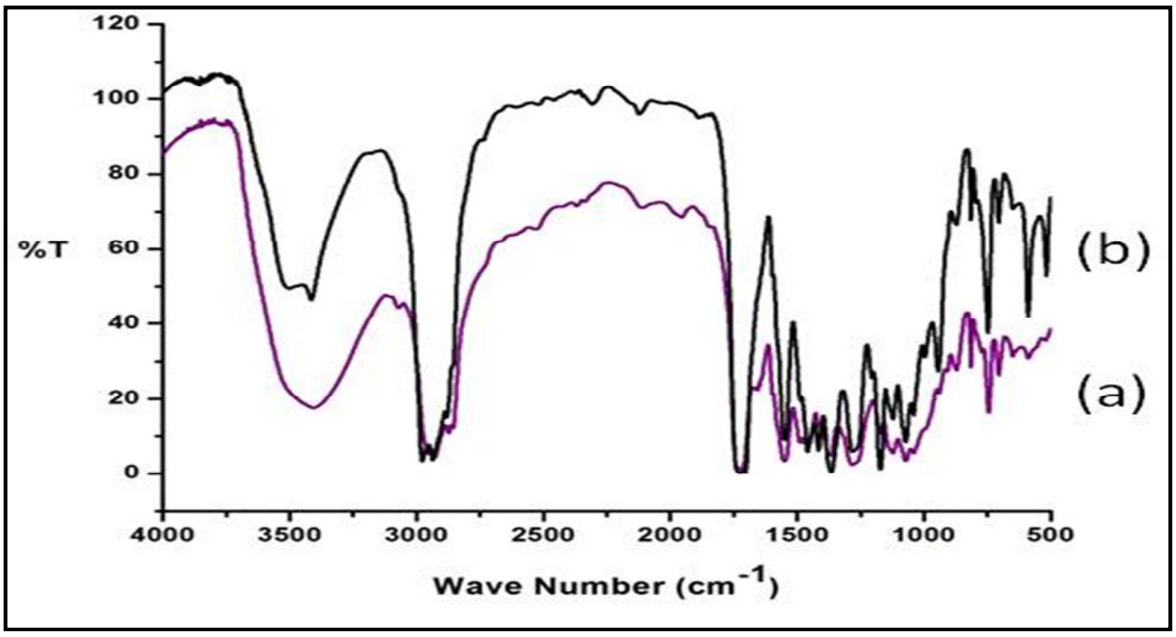

Fig. 2 FTIR spectra of: (a) SA-BMF and (b) SA-BMF-Fe_3O_4-2.5

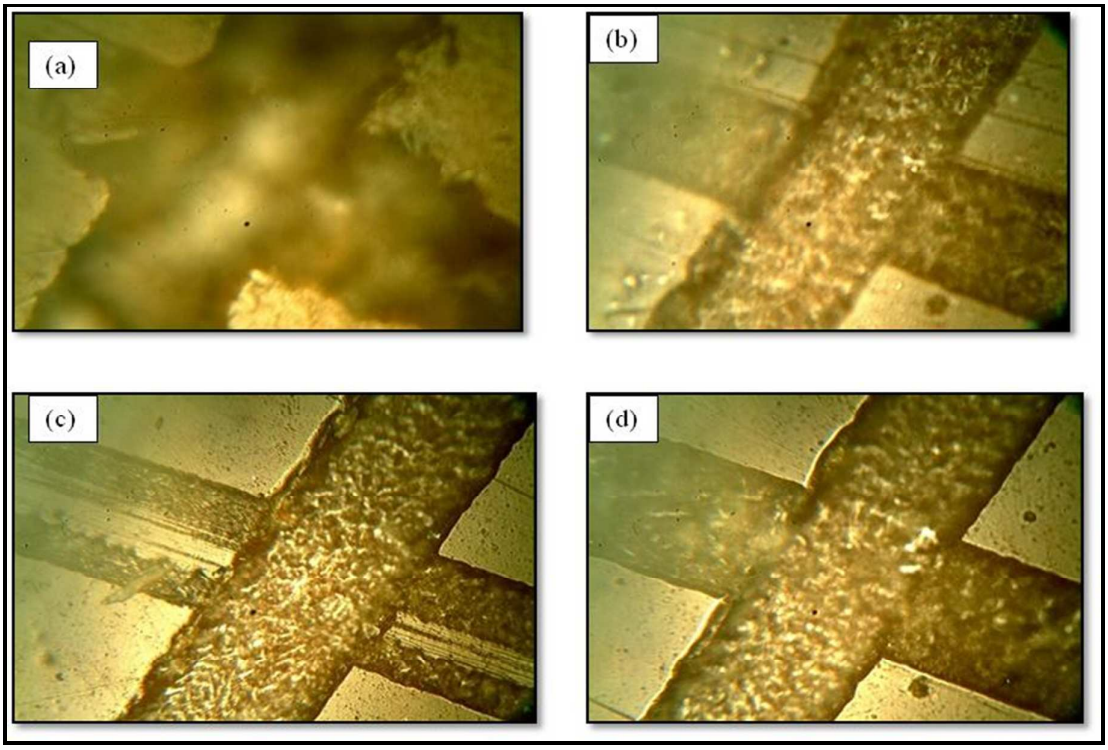

Fig. 3 Optical images of scratched CS coated with (a) SA-BMF, (b) SA-BMF-Fe_3O_4-0.5, (c) SA-BMF-Fe_3O_4-1.5 and (d) SA-BMF-Fe_3O_4-2.5 at 100× before corrosion test.

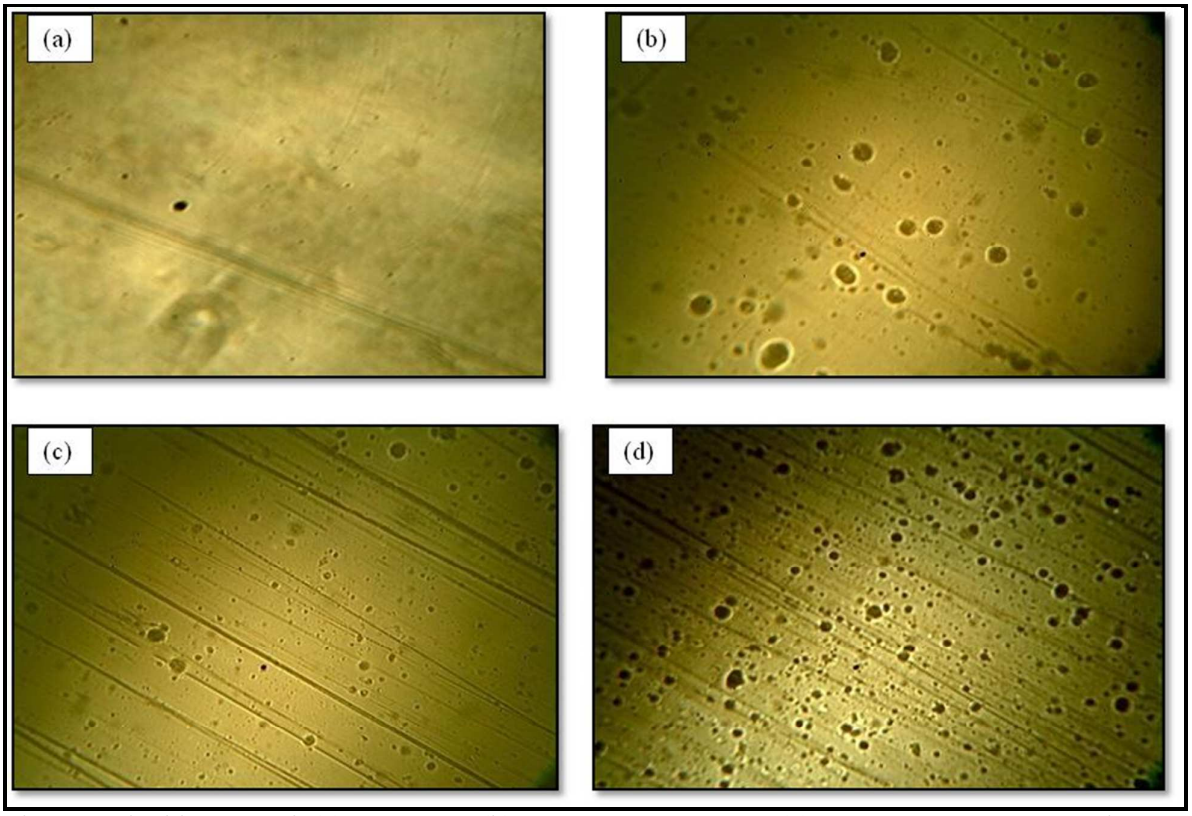

Fig. 4 Optical images of: (a) SA-BMF, (b) SA-BMF-Fe_3O_4-0.5, (c) SA-BMF-Fe_3O_4-1.5 and (d) SA-BMF-Fe_3O_4-2.5

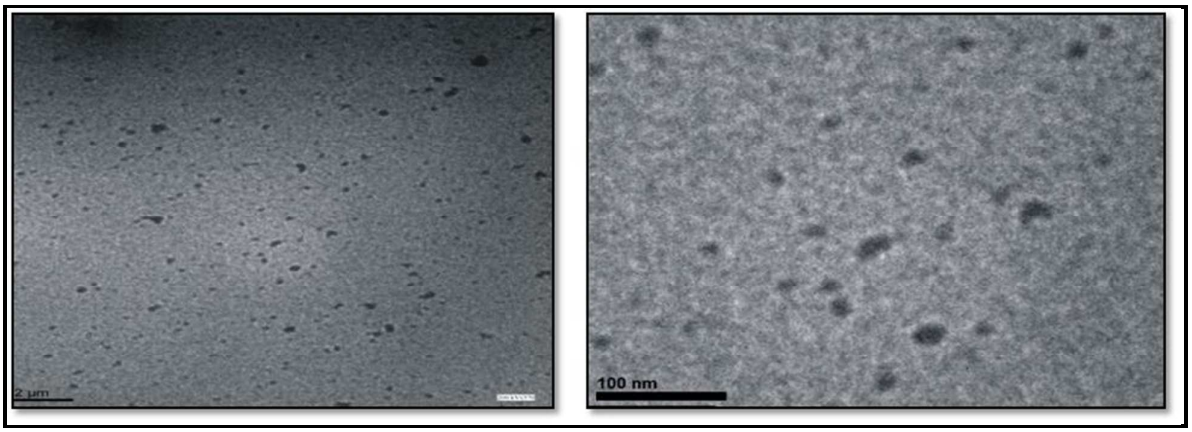

Fig. 5 TEM micrographs of SA-BMF-Fe_3O_4-2.5

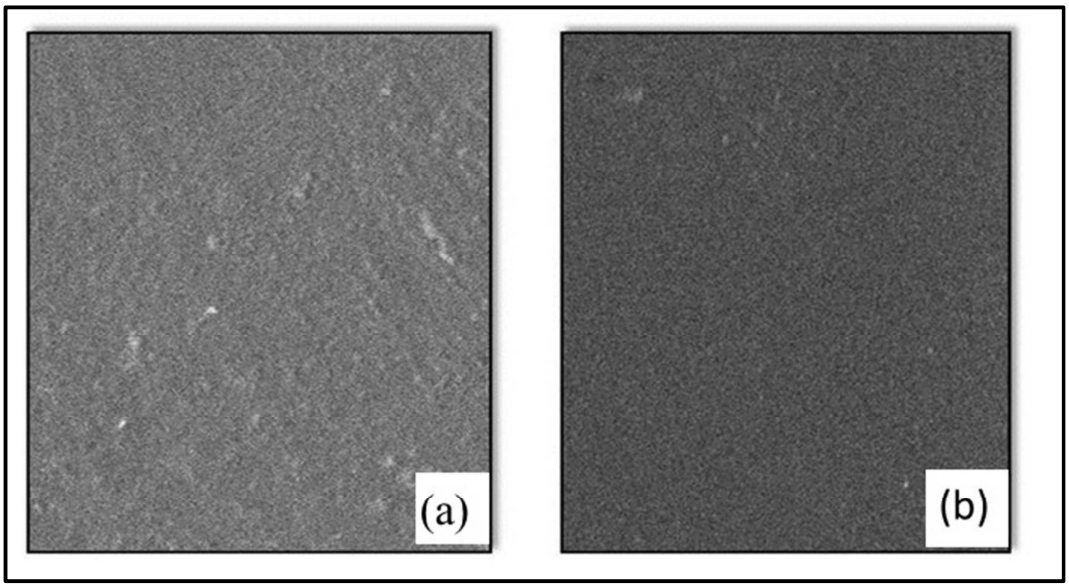

Fig. 6 SEM micrograph of (a) SA-BMF and (b) SA-BMF-Fe_3O_4 nanocomposite

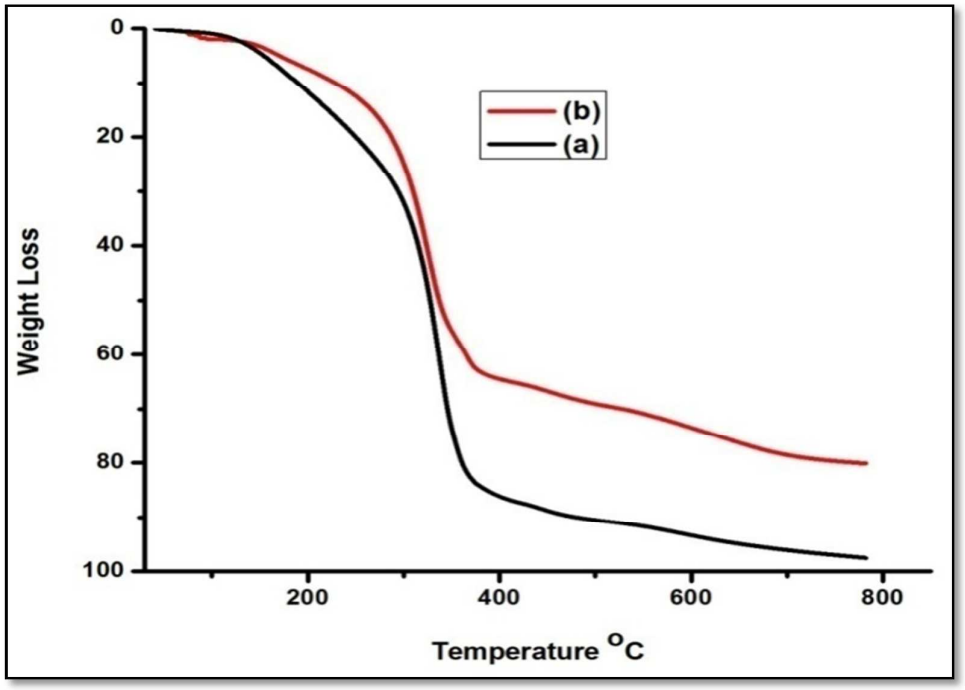

Fig. 7 TGA thermogram of (a) SA-BMF and (b) SA-BMF-Fe_3O_4-2.5

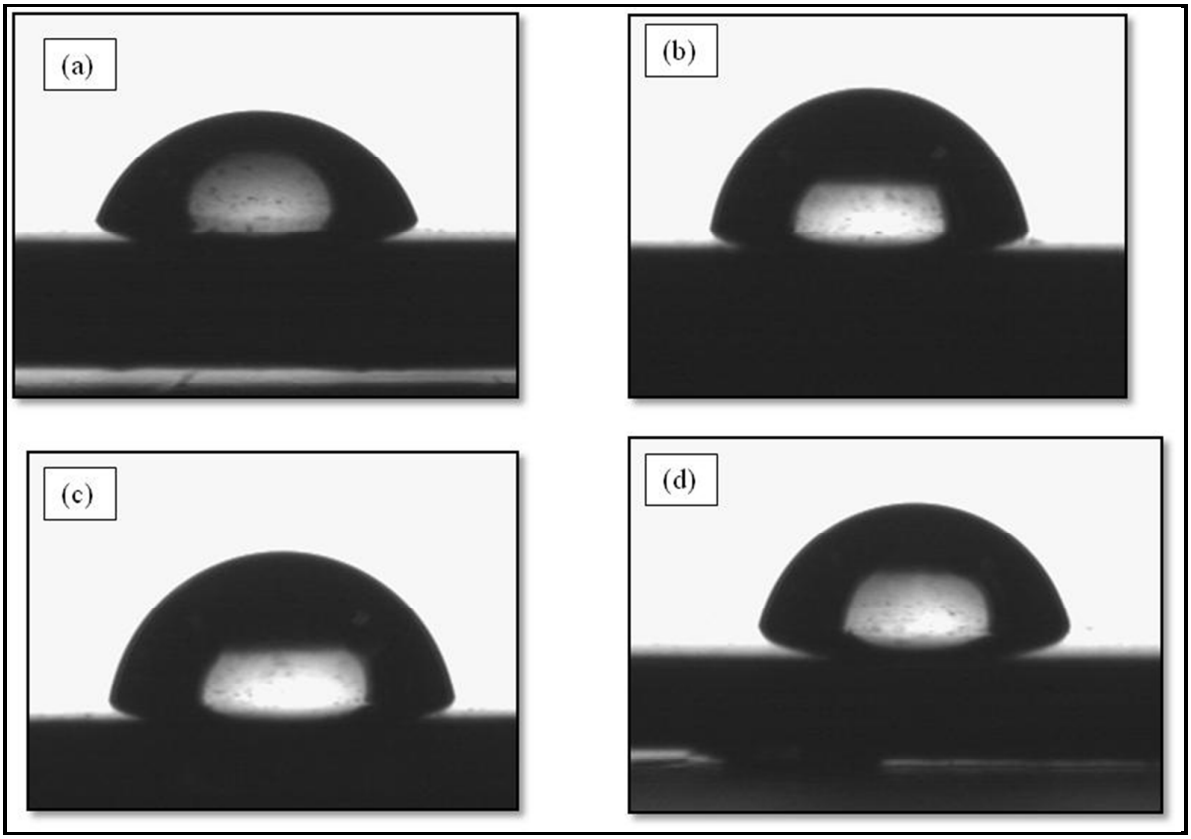

Fig. 8 Contact angle images of: (a) SA-BMF, (b) SA-BMF-Fe_3O_4-0.5, (c) SA-BMF-Fe_3O_4-1.5 and (d) SA-BMF-Fe_3O_4-2.5

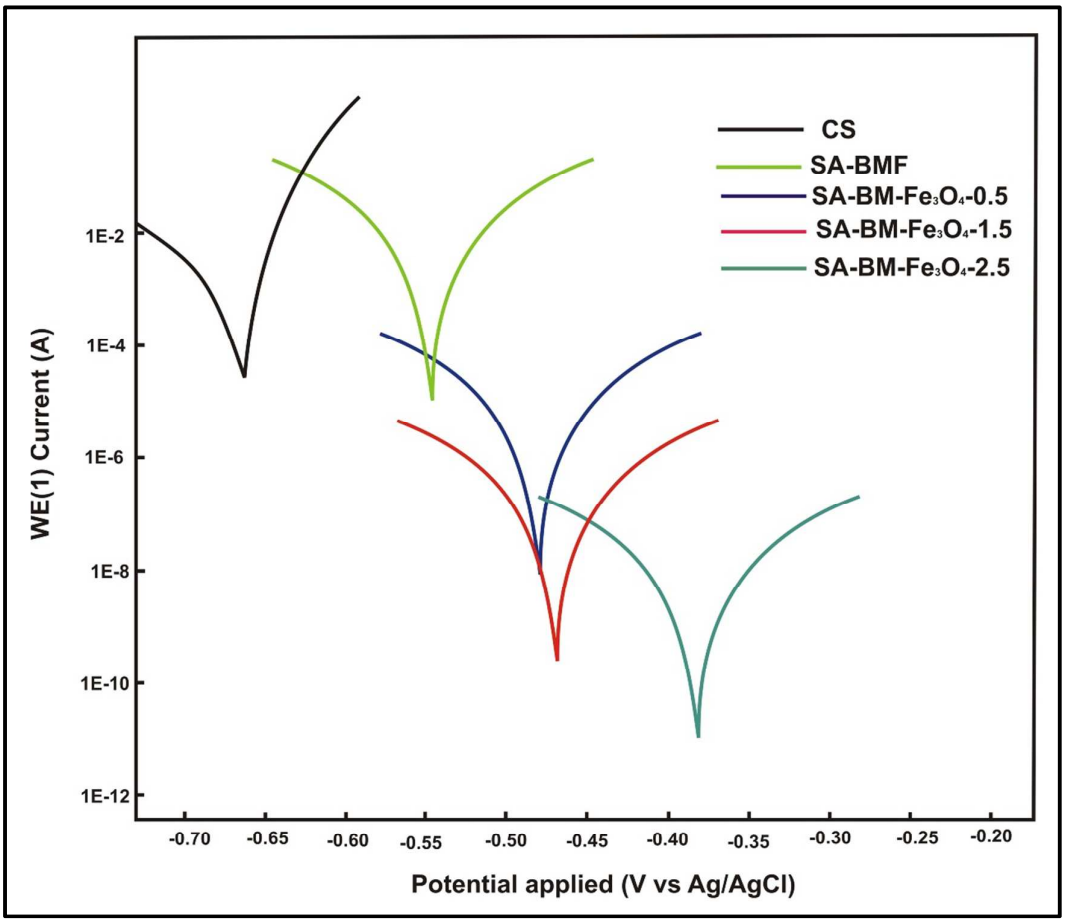

Fig. 9 Potentiodynamic polarization curve

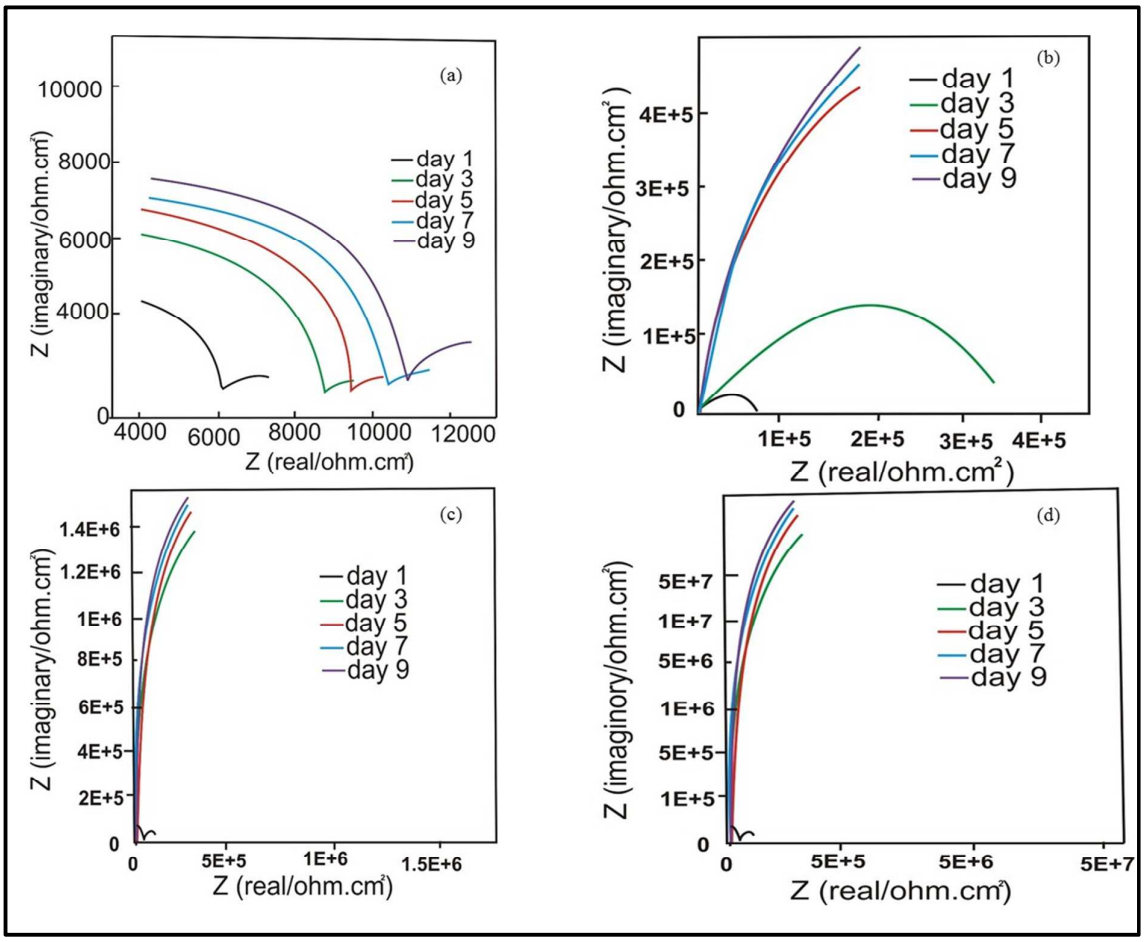

Fig. 10 Nyquist plot in 3.5 wt % NaCl solution of: (a) SA-BMF (b) SA-BMF-Fe_3O_4-0.5 (c) SA-BMF-Fe_3O_4-1.5, (d) SA-BMF-Fe_3O_4-2.5

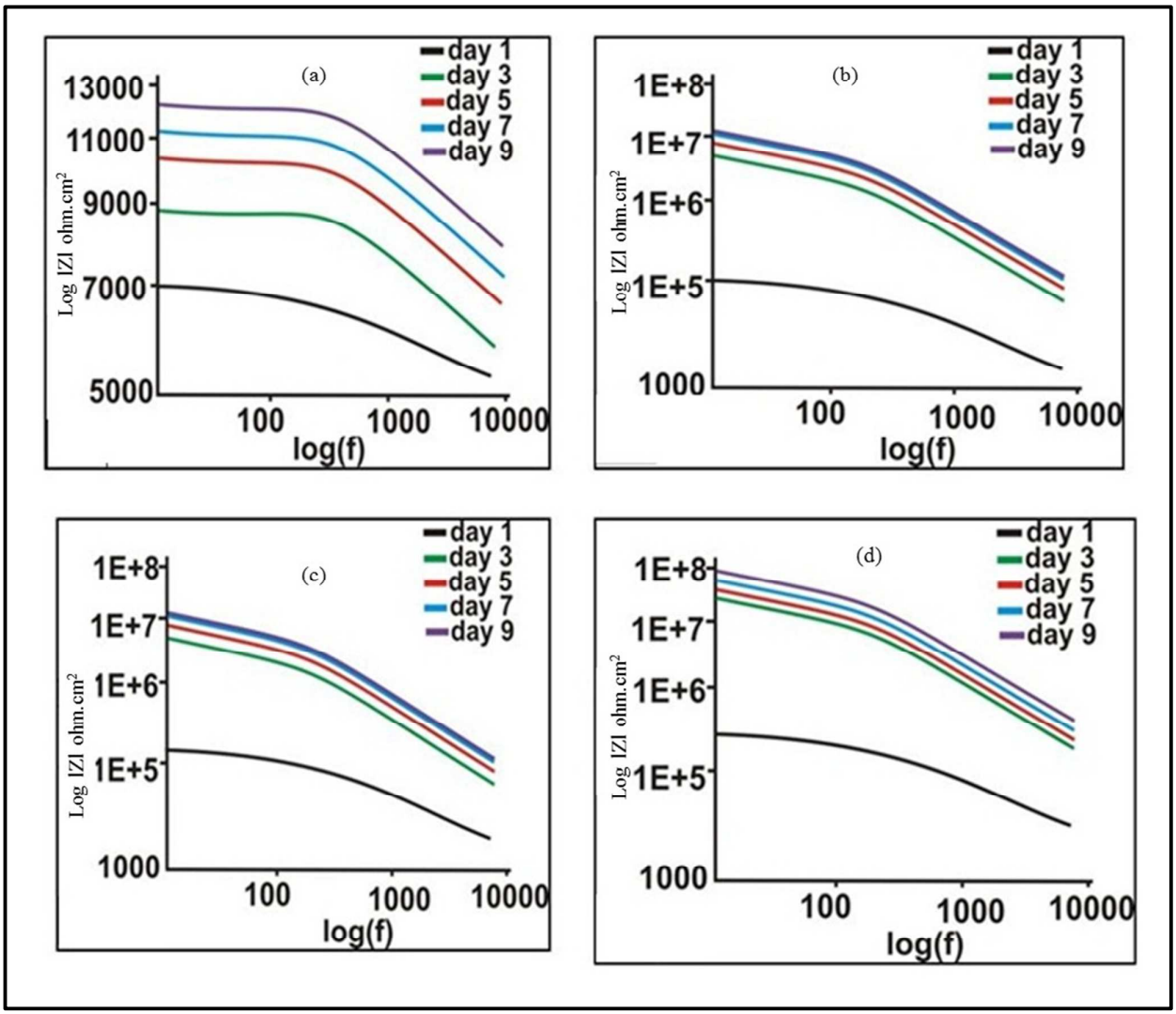

Fig. 11 Bode plot in 3.5 wt % NaCl solution of SA-BMF and nanocomposite coated samples

(a) SA-BMF (b) BMF-Fe_3O_4-0.5(c) SA-BMF-Fe_3O_4-1.5 (d) BMF-Fe_3O_4-2.5

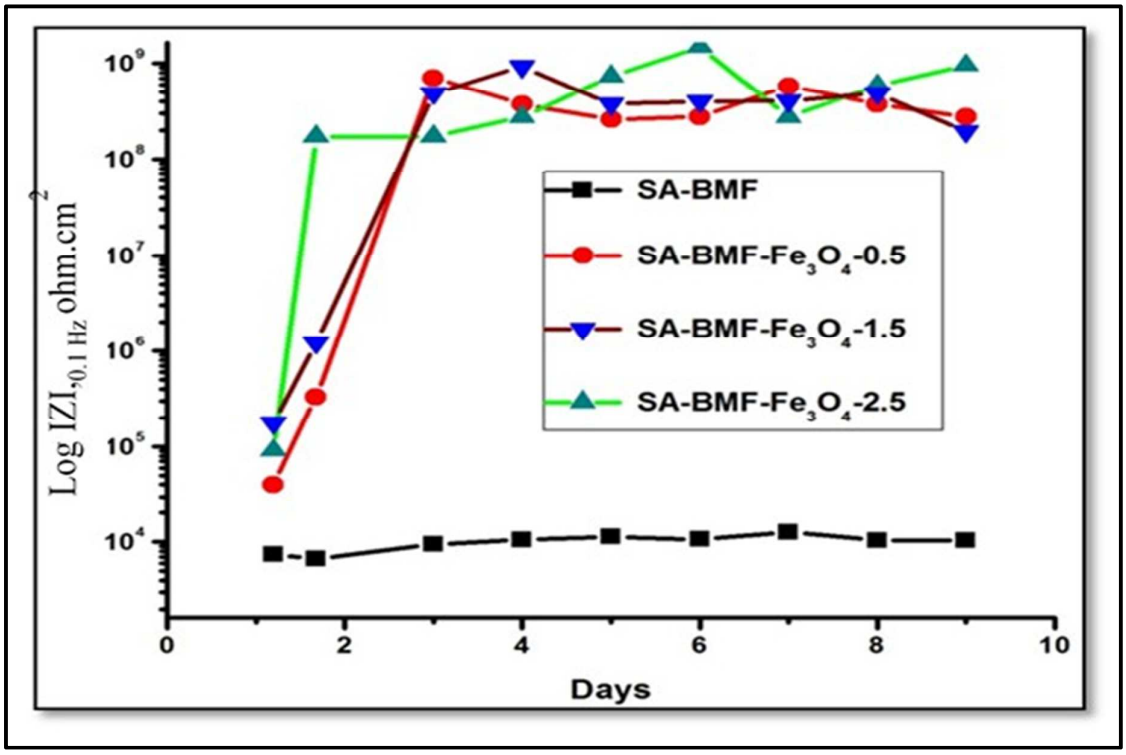

Fig. 12 $\log|Z|_{0.1Hz}$ vs exposure time for SA-BMF and SA-BMF-Fe_3O_4 nanocomposite coated samples during exposure to 3.5 wt % NaCl

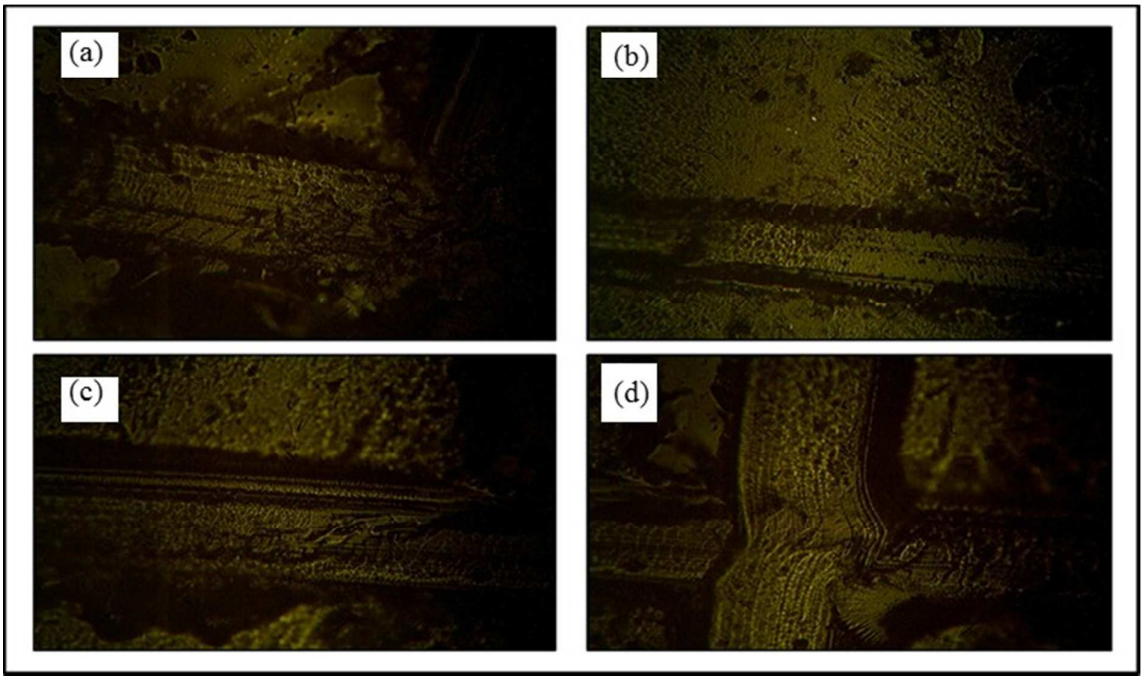

Fig. 13 (a) SA-BMF, (a) SA-BMF-Fe_3O_4-0.5, (c) SA-BMF-Fe_3O_4-1.5 and (d) SA-BMF-Fe_3O_4-2.5 at 200× after corrosion test

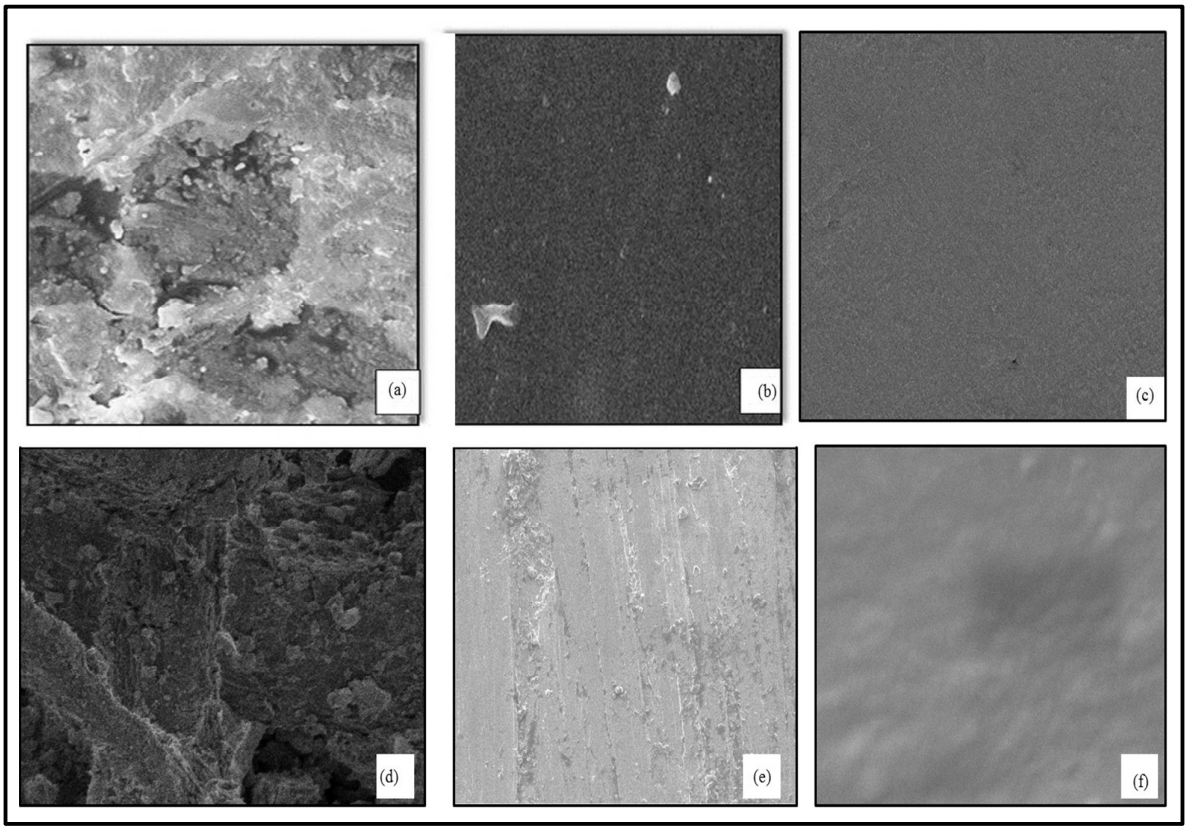

Fig. 14 SEM Images after corrosion test: (a) SA-BMF coated after 25 days, (b) SA-BMF-Fe_3O_4-2.5 coated after 25 days (c) CS uncorroded, (d) CS Corroded after 25 days, (e) SA-BMF corroded CS after removal of coating after 25 days and (e) SA-BMF-Fe_3O_4-2.5 after removal of coating after 25 days

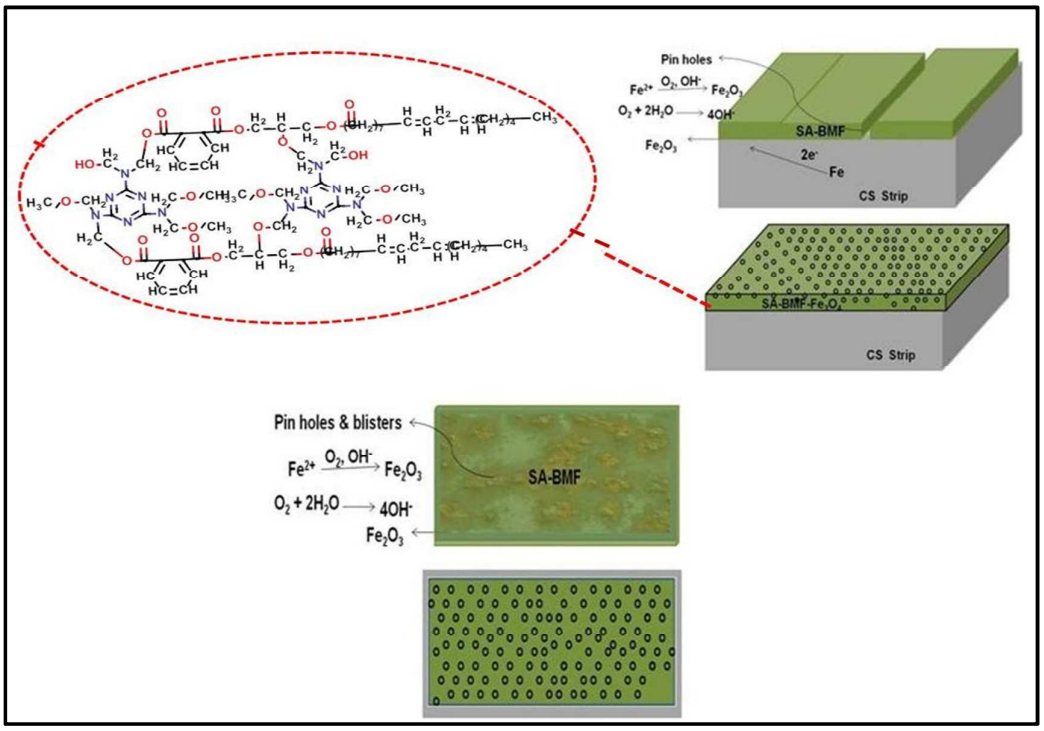

Scheme 2 Mechanism of corrosion inhibition by nanocomposite coatings

Name	Drying time (h)		Scratch Hardness (kg)	Impact Resistance (Kg/cm^2)	Refractive Index	Gloss (at 45°)	Flexibility (1/8') (Conical mandrel)
	DTT	DTH					
SA-BMF	0.50	96	4.5	Pass	1.58	80	Pass
SA-BMF-Fe_3O_4-0.5	0.25	72	10.0	Pass	1.55	75	Pass
SA-BMF-Fe_3O_4-1.5	0.20	48	12.0	Pass	1.53	72	Pass
SA-BMF-Fe_3O_4-2.5	0.20	48	14.5	Pass	1.50	68	Pass

Table 1 Physico-mechanical properties of SA-BMF and SA-BMF- Fe_3O_4 coatings

Table 2 Corrosion resistance performance by Potentiodynamic measurements of coatings

Name	E_{corr} (V vs Ag/AgCl)	Polarization resistance (Ω)	Protection efficiency
CS	-0.670	$5.75\ E^{+02}$	--
SA-BMF	-0.552	$1.11\ E^{+04}$	94.798
SA-BMF-Fe_3O_4-0.5	-0.489	$3.87\ E^{+05}$	99.851
SA-BMF-Fe_3O_4-1.5	-0.468	$8.12\ E^{+07}$	99.999
SA-BMF-Fe_3O_4-2.5	-0.385	$1.05\ E^{+08}$	99.999